JCTC Journal of Chemical Theory and Computation

Article

Cite This: J. Chem. Theory Comput. 2018, 14, 4455−4466

pubs.acs.org/JCTC

Firefly Algorithm Applied to Noncollinear Magnetic Phase Materials Prediction

Adam Payne,*[,†] Guillermo Avendaño-Franco,[†] Eric Bousquet,[‡] and Aldo H. Romero[†,§]

[†]Department of Physics, West Virginia University, Morgantown, West Virginia 26506, United States

[‡]Physique Théorique des Matériaux, CESAM, Université de Liége, B-4000 Sart Tilman, Belgium

[§]Facultad de Ingeniería, Benemérita Universidad Autonóma de Puebla, 72570 Puebla, Puebla, México

ABSTRACT: In most noncollinear crystal magnets, the number of metastable states is quite large and any calculation that tries to predict the ground state can fall into one of the possible metastable phases. In this work, we generalize the population based meta-heuristic firefly algorithm to the problem of the noncollinear magnetic phase ground state prediction within density functional theory (DFT). We extend the different steps in the firefly algorithm to this specific problem by using polarized constrained DFT calculations, whereby using Lagrange multipliers the directions of the atom magnetic moments remain fixed. By locking the directions of the magnetic moments at each search iteration, the method allows one to explore the entire Born−Oppenheimer energy surface of existing and physically plausible noncollinear configurations present in a crystal. We demonstrate that the number of minima can be large, which restrains the use of exhaustive searches.

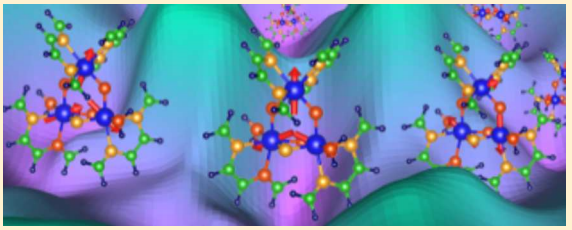

1. INTRODUCTION

Author: The construction of our modern society is strongly linked to the development of new technologies. Therefore, rapid discovery of new material systems with properties tailored to solve particular technological problems is necessary to meet this demand. Thanks so far to ever-increasing computational power, the discovery and prediction of these materials can now rely on the computer before they are synthesized in the laboratory.[1] One approach to this problem is the targeted exploration of a system's configuration space by detailing the possible minima configurations present in the Born−Oppenheimer surface. Since the minima of this space correspond to physically stable states, the goal of this approach is to locate the global minimum, as this corresponds to the ground state of the system. Even if the solution to this problem seems trivial, locating the minima of a high-dimensional surface is a highly nontrivial task. As such, a multitude of methods such as genetic algorithms, basin hopping, and random search methods, etc., have been developed to explore this space and identify minima.[2−7] However, these methods have only been applied to the problem of structural prediction.[8] The idea of optimizing physical properties other than atomic positions has also been used, as the work presented in ref 9, where a genetic algorithm to optimize the band structure of silicon and germanium semiconductors has been implemented. In that work, an undiscovered direct band gap was found. However, to the limit of our knowledge, these methods have not been applied to optimize magnetic properties, which we propose to explore in this work with noncollinear magnetism.

The magnetic properties of materials are a particularly enticing application for global search methods, from both technological and physical standpoints. Technologically, novel magnetic states could prove to be useful for next-generation storage devices. From the standpoint of basic physics, noncollinear magnetic states are of particular interest since they arise from electron correlation effects, spin−orbit coupling (SOC), surface broken symmetries, and/or geometric frustration in strongly correlated materials (SCMs).[10] On top of the exchange−correlation functional problem, studying the possible magnetic phases of noncollinear magnetic materials with DFT had limited success. This is due to the large number of metastable states that common self-consistent algorithms, such as DFT+U with spin−orbit, fail to handle when the ground state has to be identified.[11,12] Performing a calculation with initial conditions that correspond to a random point on the potential energy surface (PES) could end in any of these minima, be it a fictitious minima from the method or a minima which has a physical meaning. Additionally, these minima are very close in energy when compared to the ground state. Thus, identifying and differentiating between these minima are vital to the prediction of the correct magnetic ground state.

Meta-heuristics algorithms can provide a solution to this multiple minima problem. Meta-heuristics are general strategies to find optimal solutions of a problem by efficiently searching over the landscape of possible solutions.[13] In general, they provide rules for both crystal modifications to different states in the configuration space as well as evaluating how optimal a state is. In other words, they are used to show how energetically favorable a state is. Since they do not depend on particular details of a system, this means they can be applied to optimization of magnetic systems regardless of how the

Received: April 27, 2018
Published: July 2, 2018

DOI: 10.1021/acs.jctc.8b00404
J. Chem. Theory Comput. 2018, 14, 4455−4466

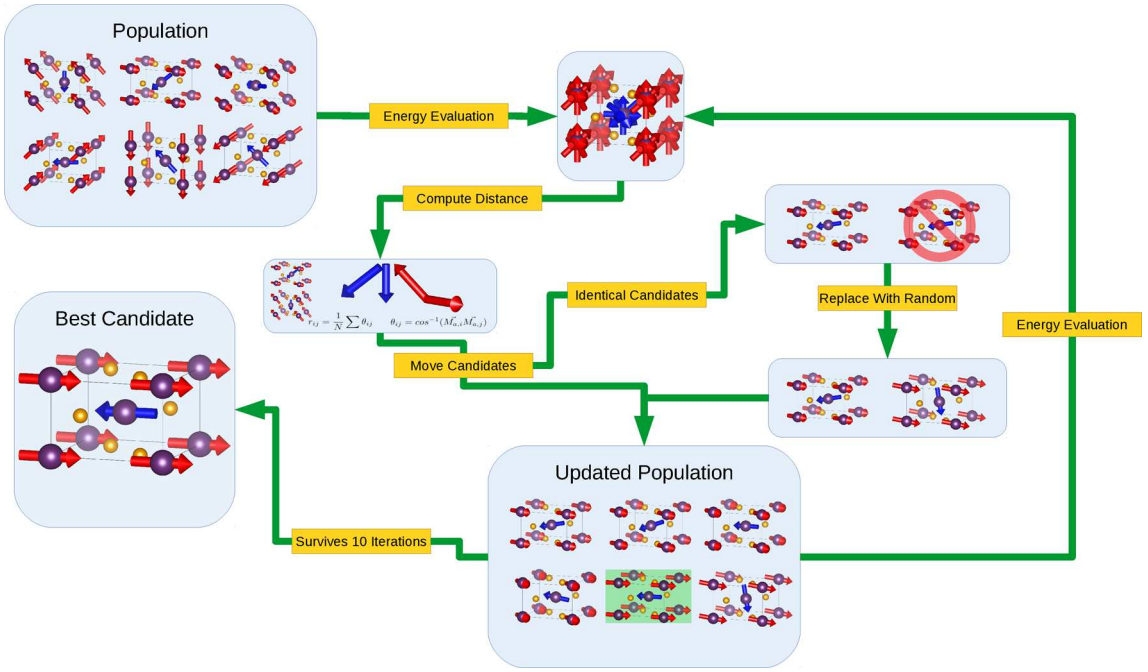

Figure 1. Firefly algorithm flowchart. Step 1 corresponds to the evaluation of the candidates' energy. After evaluation, the similarity between pairs of candidates is evaluated by using the distance function. If a candidate is identical to any other candidate, it is discarded. This corresponds to steps 3 and 4. Step 5 corresponds to when the stabilization limit is reached. This candidate is considered the ground state.

magnetism arises. In particular, a member of the subclass of population based meta-heuristics, the firefly algorithm (FA), is ideally suited to the problem at hand (this method will be discussed in more detail in section 2). We should point out that though we have limited our work to the use of DFT+U, our methodology does not rely on this approximation and can be used with any exchange−correlation functional or even different methodologies used to describe the system's magnetic properties. We will make use of DFT+U in this work, since FA does not depend on which self-consistent algorithm is used. However, we are not trying to solve the problem of the selection of the correct values of U and J, or any other problems inherent to DFT+U, in the context of ground state prediction. Rather we will show that the FA allows for the identification of the energy spectra of all local minima of a magnetic crystal and thus predicts which one has the lowest energy. Since the DFT+U approximation generates many nonphysical metastable states, it provides an ideal testing ground for FA.

The structure of this work is as follows: First, the general methodology of FA is introduced. Next, the computational details of the implementation is discussed. Then, the method is applied to three magnetic systems: NiF_2, a rutile antiferromagnetic compound which is known to display small canting away from its magnetic configuration; Mn_3Pt, a magnetic system which displays frustration and a large degeneracy of magnetic states with respect to the total energy; and a Mn model trimer $[(Mn^{IV})_3O_4L_4(H_2O)]$, where L = *N*,*N*′-bis-(methylene)-*Z*-1,2-ethenediamine, a molecular system which models the oxygen-evolving complex of photosystem II.[14] The Mn atoms are magnetic in this system, and it has recently been shown to exhibit noncollinear spin states.

2. METHODOLOGY

The firefly algorithm belongs to a class of population based meta-heuristic algorithms that aim to mimic optimization techniques used in nature.[15] As its name suggests, FA is inspired by the behavior of fireflies. In nature, fireflies are attracted to regions of space with brighter fireflies, and this attraction is modulated by the distance between these fireflies. In adapting this to magnetic materials prediction, differing magnetic moment configurations are the "fireflies", the energy of each configuration is each configuration's "brightness", and the similarity between two configurations is their "distance". Our starting point is a predefined crystal structure that will remain fixed during the magnetic phase search. A flowchart of the methodology is represented graphically in Figure 1, and the steps are summarized as follows:

1. creation of a population of random candidates, corresponding to magnetic random orientations;
2. evaluation of energies by means of DFT+U with magnetic moments constrained to the defined direction;
3. determining the distances between candidate pairs between all population elements;
4. moving candidates toward all other candidates which are lower in energy;
5. removal and replacement of identical candidates;
6. generation of new random candidates to replace identical candidates (this step completes the first generation; the process starts over on step 1 and continues until the lowest-energy candidate survives for a specified number of generations).

First, a population must be generated which correspond to a collection of magnetic moment configurations on the same crystal structure. This requires both an optimized structure as well as the identification of which atoms play a role in the magnetic properties in the system. In defining this initial population, a number of random configurations per generation

DOI: 10.1021/acs.jctc.8b00404
J. Chem. Theory Comput. 2018, 14, 4455−4466

should be specified (this step can be relaxed by allowing predefined magnetic phases as input for the initial population). If the population size is too small, the searcher will only sample a small area of the configuration space; thus there is no chance of ever finding the global minimum, unless randomness acts as the driving force of the search. With this in mind, it would seem reasonable to have as large a population size as possible. However, at a certain critical value, the searcher already samples enough of the configuration space, so nothing more is gained from the addition of more random structures. On the contrary, computational efficiency is lost. There is no general rule to determine precisely how large a population is enough. For all of our calculations using this method we have found that 16 configurations per generation strike a nice balance between sampling the configuration space and efficiency. Our initial motivation for 16 candidates is the previously application of FA to structural search.[15] Figure 2 displays the

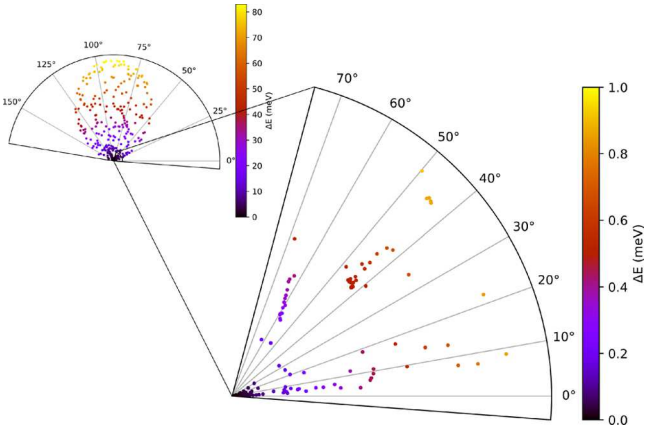

Figure 2. Polar plot of the distances and energies of all candidates relative to the lowest-energy candidate for NiF_2, with U = 4 eV and J = 0 eV. The energy is relative to the lowest-energy candidate found. The smaller plot is the plot for every candidate, and the zoomed plot is for candidates whose energy is less than 1 meV higher than the lowest-energy candidate. The distance function is defined as the average angle between magnetic sites between two candidates, so slices of constant angle correspond to candidates which are the same distance away from the lowest-energy candidate. It will be shown in a subsequent section that the minima found are all less than 1 meV in energy higher than the lowest-energy candidate. Candidates form a number of clumps in the zoomed plot; these clumps are the different minima which were located.

different minima located for NiF_2, with U = 4 eV and J = 0 eV. It can be seen that a multitude of minima were located with the use of 16 candidates per generation. Figure 3 displays both the relative energy with respect to the ground state for each candidate and a curve showing the average energy of the candidates for each generation. After 14 generations, this line stabilizes, indicating that the majority of the candidates in the subsequent generations are either in a minima or are exploring the local neighborhood around a minima. Four generations after this stabilization, the lowest-energy candidate located by the searcher is found. Together, these two plots suggest that 16 candidates per generation are sufficient.

Once the number of candidates in a given generation is defined, the population itself can be generated. To create this random population, magnetic moments with arbitrary direction are assigned to each magnetic atom. We define the magnetic moments in terms of spherical polar coordinates, so

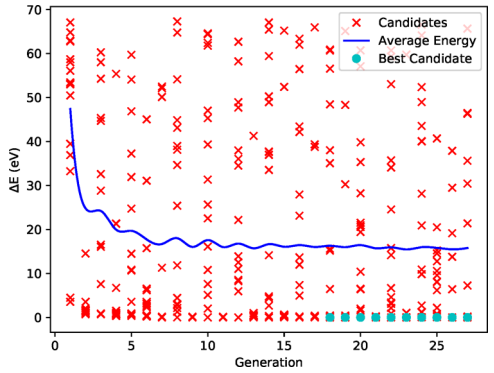

Figure 3. Relative energy of every candidate for NiF_2 with U = 4 eV and J = 0 eV with respect to the lowest-energy candidate. The blue curve is the average energy of each generation relative to the ground state. The lowest-energy candidate found is shown as well.

each angle is randomly assigned to a value from a continuous uniform distribution over their respective ranges; $[0,2\pi)$ for the azimuthal angle and $[-\pi,\pi)$ for the polar angle. The magnitude is determined from the prior optimization and remains fixed for all configurations. These randomly assigned directions remained fixed; during the static calculation of each configuration the energy is used as the criterion to rank each random configuration in terms of energetic favorability (in structural search, the enthalpy is the used quantity).

Once the total energy is calculated, each configuration evolves toward candidate configurations which are more energetically favorable. The main expression that relates the interaction between different population elements emulating the firefly behavior is given as

$$x_i^{t+1} = x_i^t + \sum_j \beta e^{-\gamma r_{ij}^2}(x_j^t - x_i^t) + \alpha_t \epsilon_t \quad (1)$$

The left-hand side of this equation, x_i^{t+1}, is the candidate in generation $t + 1$ which evolves from candidate i in generation t. The first term on the right-hand side, x_i^t, is the vector which represents the current magnetic moment of a single candidate, i, in generation t. For instance, in a system with two magnetic atoms, both of these vectors will be a six-dimensional vector, where the first three components are the Cartesian directions of the magnetic moment vector for the first atom and the last three are for the magnetic moment of the second atom. The summation in the second term is evaluated over every candidate j, which is lower in energy than i. The term $\beta e^{-\gamma r_{ij}^2}$ defines the attractiveness of firefly i to firefly j. β_0 defines the overall strength of attraction, since terms with $r_{ij} = 0$ evaluate to β_0. If $\beta_0 = 0$, the searcher becomes a random walk. γ acts as a length scale and controls the speed of convergence of the calculation. For the special case $\gamma = 0$, candidate i finds all lower-energy candidates equally attractive, and the algorithm becomes a particle swarm. The last term adds randomness to the search, where ϵ_t is a vector with components that come from a random selection of a Gaussian distribution. α_t essentially controls the amount of randomness in the searcher. The parameter r_{ij} (in eq 2) is the pairwise distance between two configurations. This parameter seeks to mimic the physical distance between two fireflies in nature.[16] In our case, physical distance is meaningless. In order to evaluate the distance between two candidate configurations, the relative angle between magnetic moment vectors on the same magnetic

DOI: 10.1021/acs.jctc.8b00404
J. Chem. Theory Comput. 2018, 14, 4455−4466

site is evaluated between the two candidates. This angle is evaluated for each magnetic site, and the average value of this angle is used as a measure of distance. The functional form of this measure is explicitly stated in eqs 2 and 3. This function is restricted to the interval $[0,\pi]$ to ensure that it is always positive.

$$r_{ij} = \frac{1}{N}\sum_{k}^{N} \theta_{ij}^{k} \tag{2}$$

$$\theta_{ij}^{k} = \cos^{-1}(\vec{M}_{k,i}\vec{M}_{k,j}) \tag{3}$$

The magnetic moments in eq 3 are normalized, and the dot product is taken between configuration i and configuration j at magnetic atom k. As this distance is evaluated pairwise between candidates, it has an index for each, i and j. The summation index, k, runs over all magnetic atoms in the system, and θ_{ij}^{k} is the angle between the magnetic moments at site k in candidates i and j. N is the total number of atoms which the summation runs over. We will now show that this definition of the distance satisfies the definition of a metric. Since a sum of metrics is also a metric, showing that the inverse cosine between a single magnetic site satisfies the definition of a metric automatically means a sum of inverse cosine function is a metric, which is the distance function defined in eq 2. For the following arguments, $d(x, y) = r_{ij} = \frac{1}{N}\sum_{k}^{N} \theta_{ij}^{k}$.

- $d(x,y) \geq 0$

The inverse cosine function can take on values in the interval $[0,\pi]$, so it is always positive.

- $d(x,y) = 0$ iff $x = y$

This is similar to the above property in that the dot product is defined on the interval $[0,\pi]$, so it only evaluates to zero if the magnetic moment configurations are identical, as this is the only case where the angle between moments on each site is zero.

- $d(x,y) = d(y,x)$

This property is satisfied since the dot product is commutative. Thus, changing the order in which the dot product is evaluated does not change the inverse cosine of this dot product.

- $d(x,z) \leq d(x,y) + d(y,z)$

Consider three unit vectors **x**, **y**, and **z**. These vectors map to points on the unit sphere. These points can be connected to form a triangle. Since the legs form a triangle, they clearly satisfy the triangle inequality. The legs of this triangle are directly proportional to the angle between the vectors which comprise its end points, meaning there is a mapping from the length of the leg to the angle between the two vectors. Thus, the angles themselves must also satisfy the triangle inequality. Therefore, our choice of distance function satisfies the definition of a metric.

Once this distance function is evaluated, each candidate is moved toward every other candidate that is lower in energy. The lowest-energy candidate remains unmodified, as it has no lower-energy candidates to move toward. It is simply promoted to the next generation within an elitism rule. Additionally, candidates which are degenerate in energy will not be moved toward one another, as candidates with the same energy are not attracted toward one another. This is why FA is ideal for multimodal problems, as different degenerate configurations do not mix with another, which means each can be found simultaneously. After this movement, the distance function is evaluated once more and identical candidates are discarded. They are in turn replaced with new random candidates so that the number of candidates per generation remains fixed. These new random candidates as well as the moved candidates are once more subjected to a static calculation, and the process begins anew. This process is continued until the lowest-energy candidate survives for a set number of generations, known as the stabilization limit. Just like the number of candidates per generation, if this number is too small, the global minimum may never be found, as the configuration space is only being sampled in a small region whenever the searcher stops. If it is too large, the searcher will continue even after the global minimum is found. We have found that a stabilization limit of 10 generations is a nice balance between these two extremes. In ref 15, the method has been applied to perform a structural search, but in this work we have generalized the implementation to include the optimization of the energy with respect to the magnetic phase. The candidate that survives this process is called the best candidate, and if the searcher parameters are properly specified so that the configuration space is appropriately sampled, this will be the ground state magnetic configuration.

3. COMPUTATIONAL DETAILS

FA has been implemented in the PyChemia package,[17] an open-source software package for materials discovery using meta-heuristic methods, which is used to perform the global search over the configuration space. This package allows flexible generation of randomly oriented magnetic moment configurations and implements the search as described in section 2. The parameters in eq 1 are necessary for the FA to operate. For all calculations we use $\beta = 0.8$, $\gamma = 0.3$, and $\alpha = 0$. Setting $\alpha = 0$ does not significantly modify FA, as only the first term on the right-hand side of eq 1 encodes the rules of the firefly meta-heuristic. Each parameter was chosen based on the work of ref 15.

The evaluation of the objective function, which is the energy of each configuration, is carried out using the Vienna ab Initio Software Package (VASP).[18−21] To take into account the interactions between the crystal structure and the spin magnetic moments, the spin−orbit coupling is turned on, which is added to the plane augmented wave Hamiltonian in a variational setup as described in ref 22. Since magnetic systems require corrections to include correlation effects, we used an extension of local density approximation (LDA) to fully capture the relevant physics. Since the magnetic atoms in each test case have localized d-electrons,[23] the LDA+U method is well-suited for evaluation of each configuration's energy. However, any particular computational method can be used for this step, as FA does not depend on the method used to evaluate energies. For all DFT calculations, we used the LDA +U method as implemented in VASP. We use the Liechtenstein approach to LDA+U, as the two commonly used approaches where the parameter J is either ignored or $J \simeq 10\%$ U are not justified in noncollinear systems.[11] The work of ref 11 shows that U acts on the electronic density, while J acts on the noncollinear magnetization densities m_x, m_y, and m_z. This does not mean that $J = 0$ cannot yield the correct magnetic ground state in noncollinear systems; it is the assumption that $J = 0$ will yield it is not valid. Additionally, to ensure that each candidate's magnetic moments remain fixed

DOI: 10.1021/acs.jctc.8b00404
J. Chem. Theory Comput. 2018, 14, 4455−4466

during energy evaluation, the constrained density functional approach, as implemented in VASP, is used.[24] This approach uses Lagrange multipliers to constrain the direction of the magnetic moments, which in turn introduces an energy penalty term in the total energy functional. The input for every constrained calculation specifies a preferred magnetic moment orientation, and the additional term in the total energy functional penalizes orientations which deviate from this preferred direction. This preferred direction is defined by a random point on the unit sphere for each magnetic atom in the system. These are randomly defined for each candidate so that each candidate has a unique magnetic moment orientation. The magnetic moment orientations must remain fixed during the calculation so that the energy of the initially defined preferred orientation is evaluated. Since there are 16 candidates per generation, this will allow for the identification of 16 different points on the PES. Since FA itself handles the movement of each candidate's magnetic moment orientation, the full relaxation of the magnetic moment directions in VASP is not necessary to explore the PES. Thus, FA determines how these 16 initial points on the PES are moved to other points on the PES. In order to force this constraint to hold, the value of the weight of the Lagrange multiplier must be specified. In the VASP code, this is denoted by the flag λ, and a value of $\lambda = 10$ was found to keep the magnetic moments constrained in the three systems we considered. However, LDA+U, as implemented in VASP, does not support the use of noncollinear kernels. It is emphasized that noncollinearity rises from the spin−orbit interaction; LDA+U is merely used to correct the correlation effects. Through the inclusion of spin−orbit coupling in our calculations, noncollinear states can still be found.[25]

The projector augmented wave (PAW) pseudopotentials as supplied with VASP were used for all elements so that spin−orbit coupling can be included, and noncollinear calculations can be performed.[26,27] An energy cutoff of 800 eV and a 6 × 6 × 10 Monkhorst−Pack k-point grid were used to ensure convergence to 10^{-8} eV, which is below the energy difference between magnetic configurations in NiF_2. In Mn_3Pt, a 16 × 16 × 16 Monkhorst−Pack k-point grid and an energy cutoff of 800 eV were used to ensure convergence to 10^{-8} eV. For $(Mn^{IV})_3O_4L_4(H_2O)$ molecule, a unit cell of 30 × 30 × 35 Å^3 was constructed to break the periodicity inherent to VASP. As it is a molecular system, a single γ point was used.

We note that the magnetic search relies on the interface created in the PyChemia package and it can be easily generalized to any other DFT code that has the constrained magnetization implementation, for example, ABINIT[28,29] or Elk.[30]

4. RESULTS

4.1. NiF_2. Our first application is for the prediction of the noncollinear ground state of NiF_2. This well-studied material has been shown experimentally to be antiferromagnetic with spin canting along the c-axis that drives weak ferromagnetism in this direction.[31,32] This canting is very small and has been measured to be 0.5°,[31] 0.38°,[33] and 2.5°.[34] The canting is believed to arise from the magnetocrystalline anisotropy (MCA).[35] Since LDA+U is used for all calculations, the results should be compared with the experiments, as energies cannot be compared between differing values of U and J. While the MCA energy has never been measured experimentally, theoretically it has been found to vary between 200 and 300 μeV depending on the values of U and J which are used.[11] Additionally, it has a bandgap of 6.5 eV[36] and an atomic magnetic moment of 2.213 ± 0.012 μ_B.[37] Our challenge is to show that our method can locate the multitude of minima which lie in the PES and compare them with experimental results. The firefly searcher was run with 16 candidates per generation, with a stabilization limit of 10 generations. We performed this search for values of U = 1.0, 2.0, 3.0, 4.0, 5.0, and 6.0 eV and J = 0.0 and 1.0 eV with $U > J$. The results in terms of canting angles for this search are listed in Table 1.

Table 1. Canting Angle and Energies of Best Candidates for All Values of U and J Considered for NiF_2 after Relaxation

U (eV)	J (eV)	canting angle (deg)
0.0	0.0	0.000
1.0	0.0	0.036
1.5	0.0	0.050
1.5	1.0	0.078
2.0	0.0	0.031
2.0	1.0	0.122
2.5	0.0	0.069
3.0	0.0	0.067
3.0	1.0	0.048
3.5	0.0	0.073
4.0	0.0	0.088
4.0	1.0	0.247
4.5	0.0	0.109
5.0	0.0	0.122
5.0	1.0	0.327
5.5	0.0	0.205
6.0	1.0	0.425

Before any physics is discussed, we stress that the FA works as intended. First we have to show that the searcher actually explores a significant region of the PES. Second, we have to show that this exploration is both targeted and is fundamentally different than that of a random search. Finally, as the generation increases, we have to show that the energy of the low-energy candidate decreases until a lowest-energy candidate is found.

Figure 4 shows the initial canting angles and angles with respect to the x-axis of each candidate for U = 2 eV and J = 0 eV. It is clear that the searcher explored a large region of the

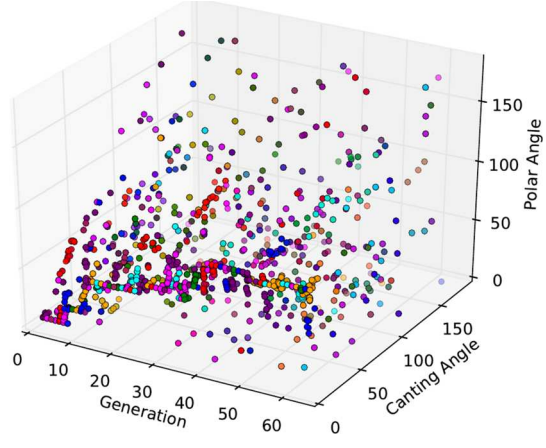

Figure 4. Initial magnetic moment configurations of candidates evaluated for U = 2 eV and J = 0.6 eV.

DOI: 10.1021/acs.jctc.8b00404
J. Chem. Theory Comput. 2018, 14, 4455−4466

PES. Figure 5 displays the targeted nature of FA more convincingly. Each node represents a single candidate; that is, each node corresponds to a unique point on the PES. For this case, there were 563 unique candidates evaluated. The blue regions correspond to the lowest-energy candidates evaluated. If two nodes are linked, that means that their magnetic moment orientations are similar to one another. If a node is not linked, this means that the magnetic moment configuration which corresponds to the node is not similar to any other candidate configuration. While the searcher does explore a large region, i.e., there are many disconnected points, the density of points near the minima is significantly greater. The degree of connectedness of a plot can be numerically evaluated. Here we use the average connectivity, which is the average of the maximum number of disjoint paths between nodes.[38] For this plot, the average connectivity is 0.229. This is because FA prefers to probe the PES near minima. From this figure, it can be seen that there are three regions which have been extensively explored.

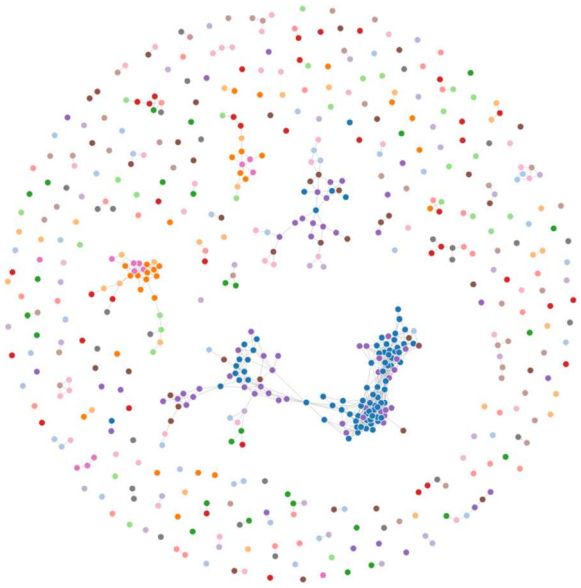

Figure 5. Network plot of the entire search for $U = 2$ eV and $J = 0$ eV. The colors denote the energy, where blue is the lowest energy and red is the highest. If two nodes are linked, the link represents eqs 2 and 3, where $r_{ij} < 0.3$. Many of the points are disconnected from the entire plot; this means these candidates were not close to any others after the initial evaluation. These points represent the stoichiastic aspect of FA, in that they are the randomly generated initial candidates as well as the replacements when duplicates are found. The other three regions which are highly linked show us the targeted nature of FA; that is that it extensively probes the regions around low-energy candidates.

Figure 6 shows the semilog of the energy difference between the lowest-energy configuration in each generation and the overall best candidate for $J = 0$ and $J = 1$. Several things are apparent from the plot. First, the energy of the best candidate decreases in each subsequent generation. This shows two things: As the searcher evolves, better candidate magnetic configurations are found. Additionally, this means that the searcher is sampling different points in configuration space. Second, the energy differences between candidates is small, as the maximum range between the starting best candidate and final best candidate is only on the order of 10^{-1} eV. This is unsurprising, as the energy difference between configurations corresponding to different local minima is only on the order of 1 meV. In Figure 6, we see that the energy difference is less than 1 meV after 15 generations. This means that the firefly searcher has located a magnetic moment configuration with magnetic moments which are perturbed slightly from their minimum values. Since the FA efficiently searches in the local area around a candidate configuration in configuration space, it is unsurprising that once the searcher locates a candidate which is close to a minimum, it only takes a few generations to find that minimum.

After the searcher has completed, each candidate should be relaxed with the constraint removed to check if the best candidate truly lies in a minimum on the PES, as well as to see how many minima lie close to the best candidate. This is done because it is possible that FA finds low-energy candidates which lie in different basins of attraction, it may not actually reach the true minimum. However, since the goal of this method is to show that it explores the many minima on the PES, showing that the candidates that the FA generates lie in different basins is enough to show that it explores much of the PES. Figure 7 shows the energy after relaxation of the last generation for $U = 2$ eV and $J = 0.6$ eV.

To show that this minimum corresponds to the ground state, we will compare the canting angles of the best candidate

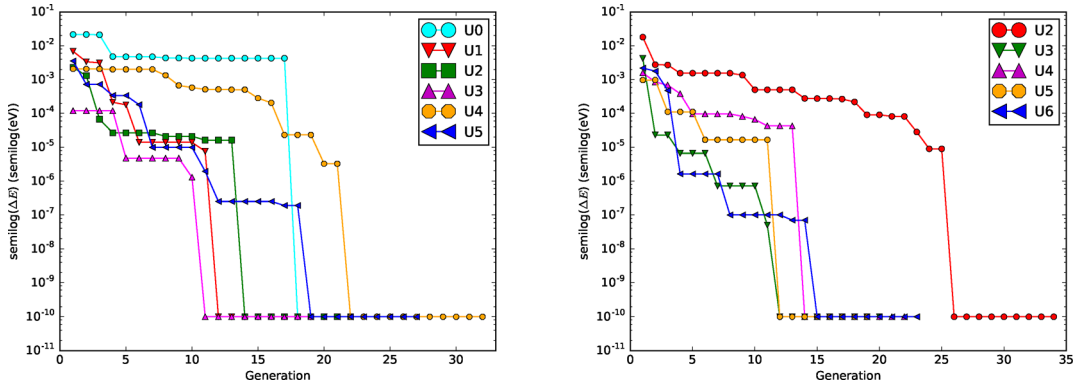

Figure 6. Energy difference between the final best candidate and the best candidate of each generation for $J = 0$ and $J = 1$ eV. This plot is logarithmic in order to show multiple values of U on the same plot. The 10 points corresponding to the 10 generations in which a structure must survive to be deemed the final best candidate are where each case plateaus. While the energy difference should be 0 eV in this case, the difference is plotted at a value which is less than the energy tolerance of every calculation. The left plot is for $J = 0$ eV; the right plot is $J = 1$ eV.

DOI: 10.1021/acs.jctc.8b00404
J. Chem. Theory Comput. 2018, 14, 4455−4466

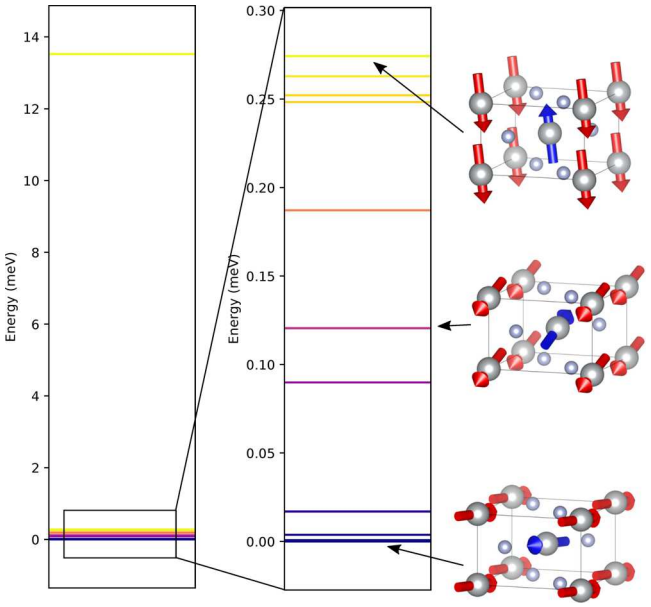

Figure 7. Energies of the last generation of candidates after relaxation for $U = 2$ eV and $J = 0.6$ eV. The left energy plot of the figure displays all of the candidates in the final generation. The middle plot is the zoomed in portion of the plot on the left. From this plot, there are three minima that are within 1^{-4} eV of the lowest-energy candidate.

that we find to the canting angles reported experimentally for NiF_2. We also compare our results to the experimentally measured bandgap and magnetic moment magnitude. Figure 8

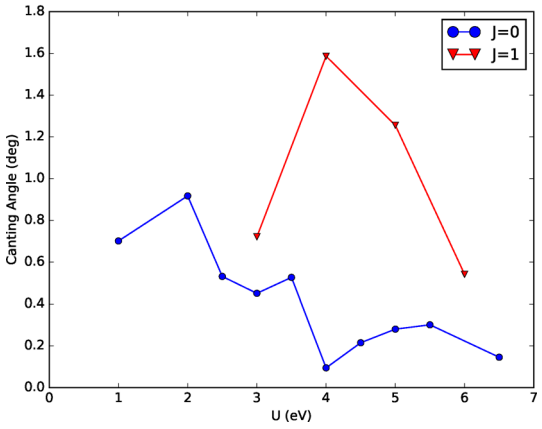

Figure 8. Canting angle for all values of U and J which have been considered, before relaxation.

shows the canting angles as a function of U for $J = 0$ and $J = 1$, before relaxation. We can see that there is no obvious trend between the value of U and the canting angle. Figure 9 shows this relationship after relaxation. This further highlights the importance of relaxation with which we see an overall trend toward an increase in the canting angle as the value of U increases. The discrepancies in this plot are due to the candidates which do not relax into the true ground state candidate.

In Figure 10 we show the energy difference between the lowest-energy candidate found for a given U for $J = 1$ and all other candidates of the same U as a function of the canting angle. The dependence between the canting angle and U is expected to be monotonic, yet the results observed in Figure 8

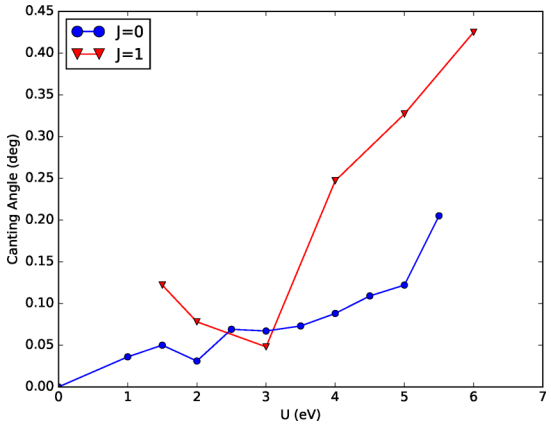

Figure 9. Canting angles for all values of U and J which have been considered after removing the constraint on the magnetic moment direction. This ensures that each candidate relaxes to a minima on the PES.

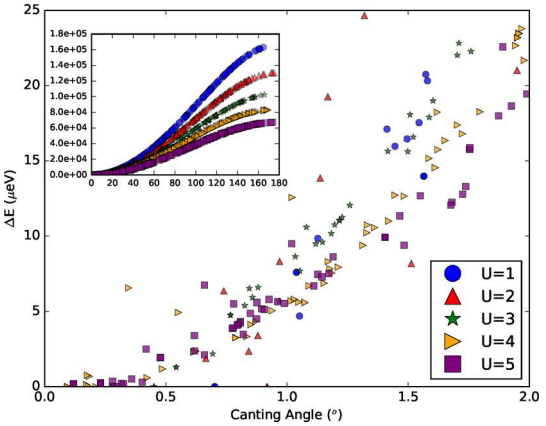

Figure 10. Energy difference for all candidates as a function of their canting angles for $J = 1$ eV (where, for example, 1.8e+05 represents 1.8×10^5).

show a dependence which is not monotonic. This is because two candidates with the same canting angle can have magnetic moments that are orientated in different directions with respect to the c-axis, which means they will have different energies after evaluation. This highlights the importance of removing the magnetic constraint, as candidates with magnetic moments that are not parallel to the c-axis will adjust their magnetic moments to lie in this plane. This is why there is such a drastic change between Figures 8 and 9.

Experimentally, the magnetic moments lie in a plane perpendicular to the c-axis.,[31,32] and the majority of the lowest-energy candidates after relaxation are in agreement with this. Each low-energy candidate has both bandgap and magnetic moments that are lower than experimentally measured values. The maximal value found for the magnetic moment is for $U = 6$ eV and $J = 1$ eV, and it is 1.76 μ_B. The maximal bandgap found was also for $U = 6$ eV and $J = 1$ eV, and it is 4.82 eV. Experimentally, these values are slightly higher than the values found, as the magnetic moment is measured to be 2.23 μ_B and the bandgap is 6.5 eV.

While our method has been able to define the lowest-energy configuration for a system with a single global minimum, i.e., in NiF_2, it is important to test that it is also able to find solutions

DOI: 10.1021/acs.jctc.8b00404
J. Chem. Theory Comput. 2018, 14, 4455−4466

which correspond to degenerate states with several and different magnetic configuration, e.g., in Mn_3Pt.

4.2. Mn_3Pt. Our second application of our FA algorithm is on Mn_3Pt. This system exhibits a first order magnetic transition between two different magnetic phases at 400 K.[39] The low-temperature phase is of interest since it is known to display frustration.[39] Neutron diffraction experiments have shown that the magnetic moments of the Mn atoms in this phase are along the [111] direction of the unit cell.[40] Additionally, the average magnetic moment of the Mn atoms is 3.0 ± 0.3 μ_B.[41]

Similarly to the previous example, we first want to show that the FA performs as intended. Figure 11 shows each different initial magnetic moment configuration evaluated for U = 4 eV and J = 0 eV. The searcher evaluated a significant portion of configuration space. Also, we can see that there are several regions where the evaluated points are very close to one another. As for NiF_2, a network plot shows the targeted nature of the FA more convincingly. We show in Figure 12 the network plot for U = 2.0 and J = 0.0. Similarly to the plot for NiF_2 each node corresponds to one candidate, and two nodes are linked only if their distance function evaluates to a value which is less than 0.3. The number of nodes in the plot is 496, which means that 496 unique candidates were evaluated. Just as before, the average connectivity can be found, and it is 0.125, which means it is less connected than the plot for NiF_2. Considering that Mn_3Pt is a frustrated system and NiF_2 is not, the graph should be more disconnected, as there should be several disconnected islands of connected nodes, with each island corresponding to a frustrated state.

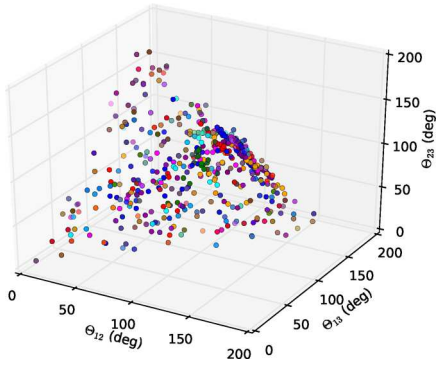

Figure 11. Initial magnetic moment configurations of candidates evaluated for U = 4 eV and J = 0 eV in Mn_3Pt. The x-axis is the angle between the first and second Mn magnetic moments, the y-axis is the angle between the first and third Mn moments, and the z-axis is the angle between the second and third Mn moments.

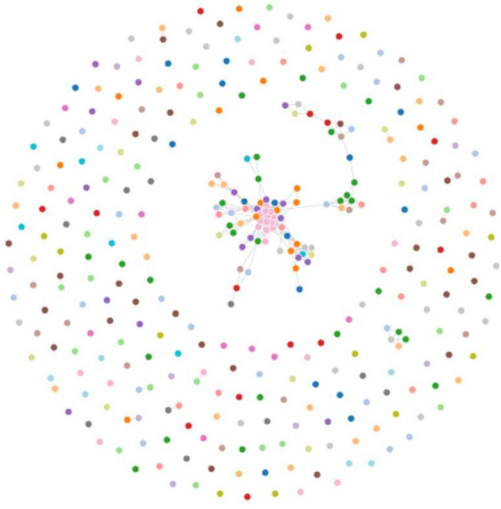

Figure 12. Network plot of the entire search for U = 4 eV and J = 0 eV in Mn_3Pt. The colors denote the energy, where blue is the lowest energy and red is the highest. If two nodes are linked, the link represents eqs 2 and (3), where r_{ij} < 0.3.

Figure 13 shows the semilog plot of the energy difference between the best candidate and the lowest-energy candidate for each generation. As expected, the energy difference decreases as the number of generations increase as the FA is locating better and better candidates as the search evolves. It is also clear that as the U value increases, the potential energy surface becomes more rough and the location of the lowest-energy configuration needs more iterations. This is consistent with the fact that as U increases, the electron−electron correlation increases, which makes magnetic energy barriers larger and the exploration of the surface more difficult, though our method is still able to find the right minima even at large U values.

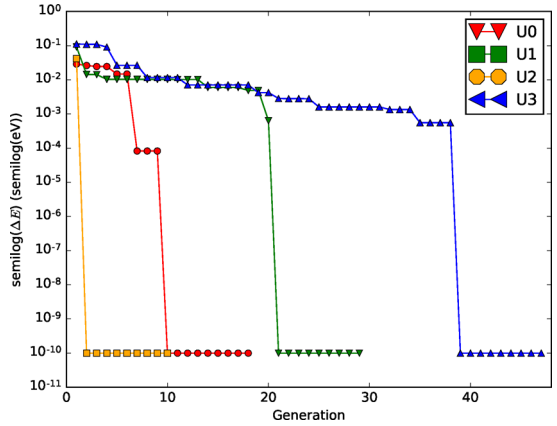

Figure 13. Energy difference between the final best candidate and the best candidate of each generation for both J = 0 in Mn_3Pt. This plot is logarithmic in order to show multiple values of U on the same plot. The nine points corresponding to the final plateau for each candidate are the best candidate. Since this is a semilog plot, the energy difference has been selected as less than that of the energy tolerance used (10^{-9} eV) to avoid infinities in the graph.

We performed the search for U values of 0.0,1.0,2.0,3.0 eV, and 4.0 eV for J = 0 eV. Figure 14 shows our results for the magnetic moment magnitudes for all low-energy candidates which have been found after relaxation. We found two cases in which two lowest-energy candidates have magnetic moment magnitudes that agree with experiment, U = 2 eV and U = 3 eV.

We also need to determine if FA yields magnetic moment orientations that agree with experiment. Figure 15 shows the magnetic moments of two candidates after relaxation, U = 2.0 and U = 1.0. Only U = 2.0 has magnetic moments which lie in the [111] plane. Combining these two results together, we find that the low-energy candidate found for U = 2 eV and J = 0 eV is consistent with experimental measurements. Additionally, previous computational studies have identified three potential

DOI: 10.1021/acs.jctc.8b00404
J. Chem. Theory Comput. 2018, 14, 4455−4466

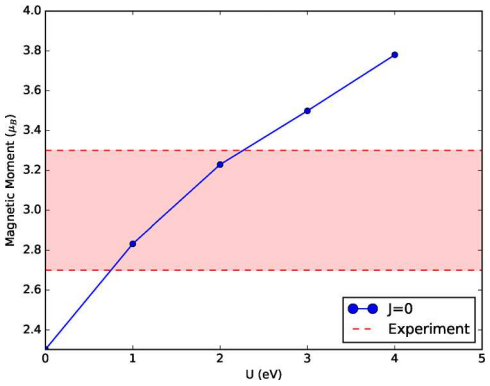

Figure 14. Average Mn magnetic moments of the lowest-energy candidates for Mn_3Pt.

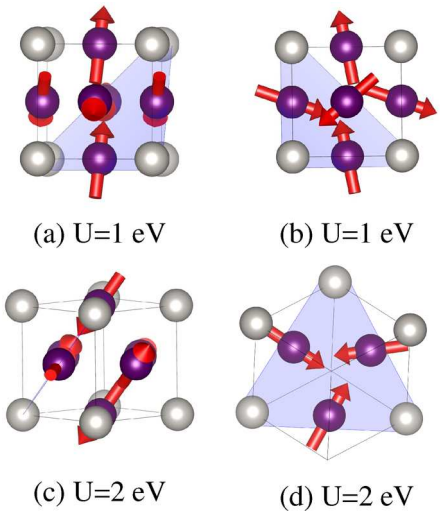

Figure 15. Magnetic moments of each low-energy candidate for Mn_3Pt. Panels a and c display the orientation of the magnetic moments relative to the [111] plane. U = 2.0 lies in this plane; U = 1.0 does not. Panels b and d display the orientations of the magnetic moments within the plane they lie in. The result for U = 2.0 agrees with both experiment and previous theoretical results.

configurations which agree with neutron diffraction experiments.[39]

The diversity of the minima of the relaxed generation can also be checked. Since the lowest-energy candidate should lie in the [111] plane, the relative orientation of the plane the magnetic moments lie in can be used to differentiate results. We show this result in Figure 16 for U = 2.0 and J = 0.0. Unsurprisingly, most of the candidates relax to a configuration which either is in the [111] plane or is close to the [111] plane. Most of the candidates lie within 0.5 meV above the lowest-energy candidate. The candidate which is 3 meV higher in energy can be identified with another theoretically predicted orientation which agrees with experiment, even though it is not exactly in the [111] plane.[39] This orientation was predicted to be 2.8 meV higher in energy than the lowest-energy orientation, a result that is in agreement with our calculations. Since Mn_3Pt is a frustrated system, there should be at least one more magnetic moment configuration which has the same energy as the lowest-energy candidate. The third configuration identified in Figure 16 is only 1 μeV higher in energy than the lowest-energy candidate. Since this energy difference is significantly lower than what was previously reported, this

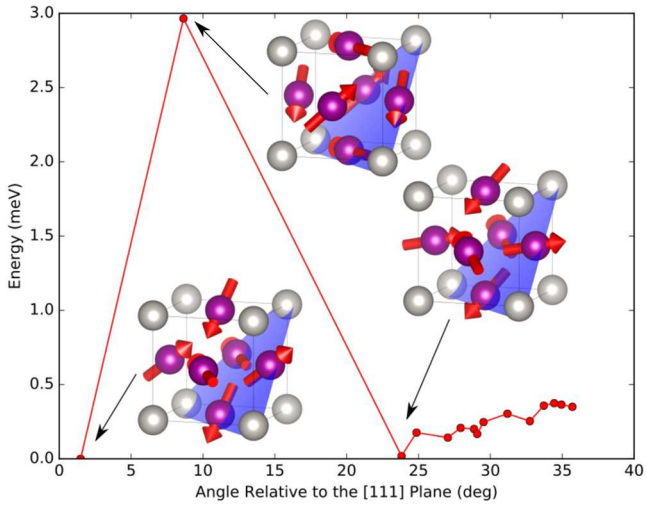

Figure 16. Relative energy of each candidate in terms of its orientation of the planes in which its magnetic moments lie after relaxation, relative to the [111] plane for Mn_3Pt. These are for the candidates in the final generation of the search for U = 2.0 and J = 0.0. There are many minima located near the lowest-energy candidate. The peak of the figure is 3 meV higher in energy than the lowest-energy configuration. This higher-energy candidate is identified as one of the three theoretically predicted orientations which agrees with experiment. The candidate which has an energy difference of 1 μeV with the lowest-energy candidate is identified as a degenerate state.

candidate is identified as a degenerate configuration. Thus, the expected degeneracy in this system has been reproduced by the FA.

4.3. $(Mn_{IV})_3O_4L_4(H_2O)$. Our final application of FA is on the molecular system $(Mn^{IV})_3O_4L_4(H_2O)$, where L = *N*,*N*′-bis(methylene)-*Z*-1,2-ethenediamine. This molecular system mimics the oxomanganese complex of photosystem II, and the action of this complex causes the oxidation of water to dioxygen. Because of this, the considered molecular system is a simplified version of the well-studied $(Mn^{IV})_3O_4(bpy)_4(H_2O)$ system.[42] This oxidation is a key step in the utilization of solar energy in biological systems. Experimental work with $(Mn^{IV})_3O_4(bpy)_4(H_2O)$ has indicated that strong antiferromagnetic coupling exists between the spin centers. The three oxomanganese complexes in this molecular system are aligned such that the Mn atoms in each complex lie on the vertices of a triangle, similarly to the case for Mn_3Pt. Because of this, it is believed that competition between the three spin centers leads to frustration. The theoretical work of Luo et al.[14] showed that if the spins of these atoms adopt a noncollinear configuration, then this frustration is minimized, resulting in a state lower in energy than the previously expected frustrated collinear configurations. Since this system has been shown previously to display a noncollinear spin arrangement, it provides a molecular system where FA can be tested. Luo et al. found a ground state configuration where the magnetic moments of the Mn atoms lie in the $x-y$ plane, where each magnetic moment points outward from the center of the triangle connecting the three Mn atoms. The energy difference between this noncollinear state and the lowest-energy collinear state is 0.3 eV. While they also considered excited states of this molecule, these are not necessary for our purposes, as we are trying to predict the ground state of the system. For our searcher, we selected U = 0, 1, and 2 eV, with J = 0 eV, based on our results for Mn_3Pt, since the Mn atoms are the magnetic atoms in both

DOI: 10.1021/acs.jctc.8b00404
J. Chem. Theory Comput. 2018, 14, 4455−4466

systems. As with the previous cases, we first want to show that a significant portion of configuration space is explored. Figure 17 displays the network plot we obtained for

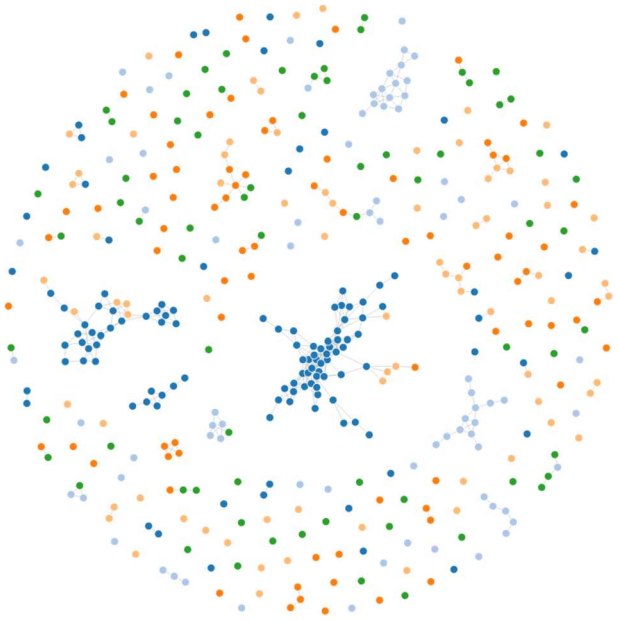

Figure 17. Network plot for the molecular system $(Mn^{IV})_3O_4L_4(H_2O)$.

$(Mn^{IV})_3O_4L_4(H_2O)$. As discussed for the previous two cases, each node corresponds to a single candidate and nodes are linked based on their distance from one another. As before, the distance cutoff was specified to be 0.3, on a scale where 0.1 specifies candidates which are identical. Since the average angles between magnetic sites are used to define the distance, this cutoff means the average angle must be less than 0.3 radians between magnetic moment sites. Just as in the previous cases, the graph is primarily a collection of completely disconnected nodes and highly connected nodes, which shows that the searcher is targeted. There are 424 nodes, which means there were 424 unique magnetic moment configurations which were evaluated by FA.

Figure 18 shows the energy difference between different candidates for the final generation for U = 2 eV and J = 0 eV. The first remark we can make is that the energy differences between minima are on the order of 0.1 meV. The second remark is that 16 different minima were located in this final generation. This, coupled with the network plot in Figure 17, shows that a calculation that starts with initial conditions that correspond to a random point on the PES has very little hope of relaxing into the global minimum.

Finally, the lowest-energy candidate has properties which agree with the results from the work of Luo et al. The magnetic moments lie in the $a-c$ plane, and they are oriented pointing outward from the center of the triangle where the Mn atoms lie on. However, our results yield magnetic moment magnitudes which are significantly higher than those previously reported. Figure 19 displays the average magnetic moment magnitude of the best candidate for the values of U and J considered, along with the value from the previous theoretical study. The disagreement between our results on the previous theoretical work is not a failure of the FA, however, but is more than likely due to our use of a different exchange−correlation functional

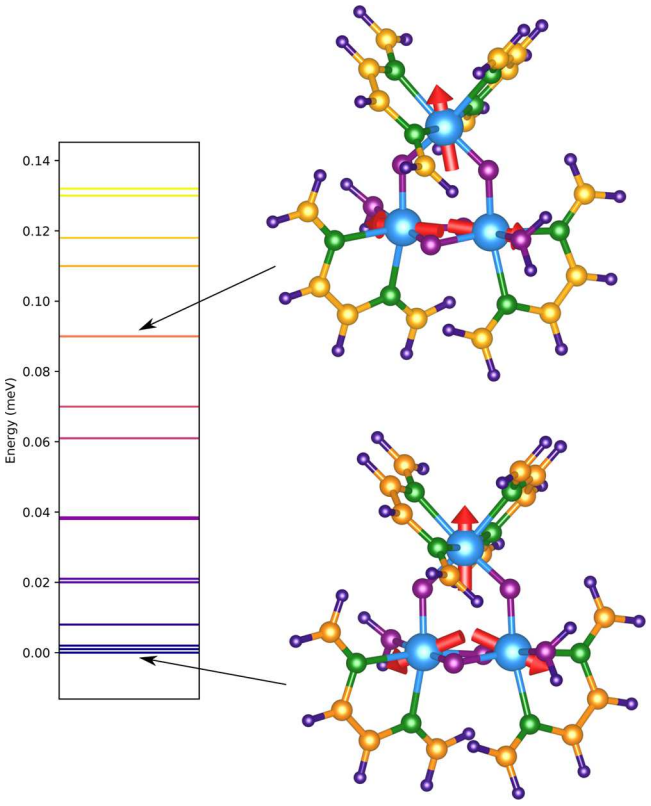

Figure 18. Energy differences between candidates in the final generation for U = 2 eV and J = 0 eV after relaxation. Each line corresponds to a different minimum.

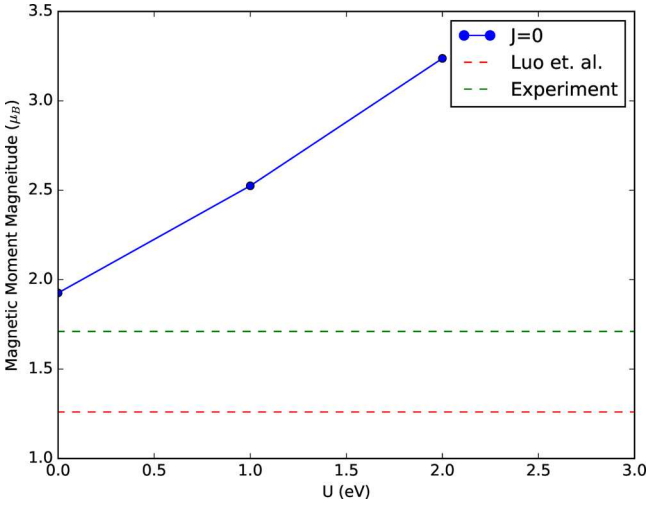

Figure 19. Average magnetic moment magnitude of the best candidate for all values of U and J considered for the molecular system. The dashed lines are the average magnetic moment values from previous theoretical and experimental work.[14,42]

as well as our use of LDA+U. Experimentally, the reported magnetic moments of $(Mn^{IV})_3O_4(bpy)_4(H_2O)$ go from 1.71 μ_B at 4.6 K to 3.77 μ_B at 292 K,[42] which is higher than those reported by Luo et al. and in better agreement with our results.

5. CONCLUSION

In this work we have shown that meta-heuristic firefly algorithm is ideally suited to the problem of ground state prediction in noncollinear magnetic systems due to its ability

DOI: 10.1021/acs.jctc.8b00404
J. Chem. Theory Comput. 2018, 14, 4455−4466

to efficiently search over multiple regions of configuration space simultaneously. It does not depend on specific details of a system, so it can be applied to a wide range of materials with wildly varying properties. Both of these reasons make it well-suited to locate the global minima of noncollinear magnetic systems. When applied to NiF_2, it has been shown that FA can yield correct values for the canting angle without taking into account crystal symmetry, the existence of MCA, nor any other specific property of NiF_2. For Mn_3Pt, not only was the FA able to locate the correct ground state magnetic moment orientation but also it was able to locate a second previously reported orientation which agrees with the experiment. Additionally, for several values of U and J, the magnetic moments were found to lie in the [111] plane before relaxation, and the correct orientation within this plane was found after relaxation. For the molecular system $(Mn^{IV})_3O_4L_4(H_2O)$, the FA algorithm was able to find a low-energy magnetic moment configuration whose orientation agrees with previous theoretical work.[14] The FA could also be used in the identification of the values of U and J which correctly reproduce the experimental noncollinear properties of crystals. More importantly, in all three cases a multitude of minima were identified, which enabled differentiation between different stable and metastable magnetic moment configurations. This improves on the weakness of current random methods, as calculations using random methods can relax into any of the numerous minima which were located using FA. It should be noted that there were approximately 500 unique candidates evaluated in each test case. While it is not necessary for FA to function properly, analysis of magnetic symmetries has been used successfully to limit the number of possible states which are physically realizable.[43] An implementation of magnetic symmetry analysis in the PyChemia package would be useful addition to limit the number of possible states.

In general, we have demonstrated that the FA is a very flexible method to be used in the search of global minima in problems where the potential energy surface is rather complex. This implementation could thus be very useful to search low-energy magnetic phases of noncollinear magnets with a larger number of cations, in particular those where there is a role between the magnetic and the electronic properties.

AUTHOR INFORMATION

Corresponding Author

*E-mail: apayne9@mix.wvu.edu.

ORCID

Adam Payne: 0000-0002-3735-0405

Funding

This work used the Extreme Science and Engineering Discovery Environment (XSEDE), which is supported by the National Science Foundation (NSF) Grant No. OCI-1053575. Additionally, we acknowledge the support from the Texas Advances Computer Center (TACC) with the supercomputer Stampede 2, Bridges supercomputer at the Pittsburgh Supercomputer Center, and Super Computing Systems (Spruce and Mountaineer) at West Virginia University (WVU). A.H.R., G.A.-F., and A.P. acknowledge the support from NSF DMREF-NSF 1434897 and the U.S. Department of Energy (DOE) DE-SC0016176 projects. E.B. acknowledges the ARC project AIMED and the F.R.S-FNRS PDR project MaRePeThe for funding. E.B. has relied on the PRACE project TheDeNoMo and on the CECI facilities funded by F.R.S-FNRS (Grant No. 2.5020.1) and the Tier-1 supercomputer of the Fédération Wallonie-Bruxelles funded by the Walloon Region (Grant No. 1117545) for simulations.

Notes

The authors declare no competing financial interest.

REFERENCES

(1) Woodley, S. M.; Catlow, R. Crystal structure prediction from first principles. *Nat. Mater.* **2008**, *7*, 937−946.

(2) Amsler, M.; Goedecker, S. Crystal structure prediction using the minima hopping method. *J. Chem. Phys.* **2010**, *133*, 224104.

(3) Wang, Y.; Lv, J.; Zhu, L.; Ma, Y. Crystal structure prediction via particle-swarm optimization. *Phys. Rev. B: Condens. Matter Mater. Phys.* **2010**, *82*, 094116.

(4) Glass, C. W.; Oganov, A. R.; Hansen, N. USPEX Evolutionary crystal structure prediction. *Comput. Phys. Commun.* **2006**, *175*, 713−720.

(5) Wales, D. J.; Doye, J. P. K. Global Optimization by Basin-Hopping and the Lowest Energy Structures of Lennard-Jones Clusters Containing up to 110 Atoms. *J. Phys. Chem. A* **1997**, *101*, 5111−5116.

(6) Tipton, W. W.; Hennig, R. G. Random Search Methods. *Modern Methods of Crystal Structure Prediction*; Wiley-VCH Verlag: Weinheim, Germany, 2011; pp 55−66, DOI: 10.1002/9783527632831.ch3.

(7) Schoen, F. Stochastic techniques for global optimization: A survey of recent advances. *J. Global Optim.* **1991**, *1*, 207−228.

(8) Oganov, A. R., Ed. *Modern Methods of Crystal Structure Prediction*, 1st ed.; Wiley-VCH Verlag: Weinheim, Germany, 2011; DOI: 10.1002/9783527632831.

(9) d'Avezac, M.; Luo, J.-W.; Chanier, T.; Zunger, A. Genetic-Algorithm Discovery of a Direct-Gap and Optically Allowed Superstructure from Indirect-Gap Si and Ge Semiconductors. *Phys. Rev. Lett.* **2012**, *108*, 027401.

(10) Dagotto, E. Complexity in Strongly Correlated Electronic Systems. *Science* **2005**, *309*, 257−262.

(11) Bousquet, E.; Spaldin, N. J dependence in the LSDA+U treatment of noncollinear magnets. *Phys. Rev. B: Condens. Matter Mater. Phys.* **2010**, *82*, 220402.

(12) Allen, J. P.; Watson, G. W. Occupation matrix control of d- and f-electron localisations using DFT + U. *Phys. Chem. Chem. Phys.* **2014**, *16*, 21016−21031.

(13) Bianchi, L.; Dorigo, M.; Gambardella, L. M.; Gutjahr, W. J. A survey on metaheuristics for stochastic combinatorial optimization. *Nat. Comput.* **2009**, *8*, 239−287.

(14) Luo, S.; Rivalta, I.; Batista, V.; Truhlar, D. G. Noncollinear Spins Provide a Self-Consistent Treatment of the Low-Spin State of a Biomimetic Oxomanganese Synthetic Trimer Inspired by the Oxygen Evolving Complex of Photosystem II. *J. Phys. Chem. Lett.* **2011**, *2*, 2629−2633.

(15) Avendaño Franco, G.; Romero, A. H. Firefly Algorithm for Structural Search. *J. Chem. Theory Comput.* **2016**, *12*, 3416−3428.

(16) Sadeghi, A.; Ghasemi, S. A.; Schaefer, B.; Mohr, S.; Lill, M. A.; Goedecker, S. Metrics for measuring distances in configuration spaces. *J. Chem. Phys.* **2013**, *139*, 184118.

(17) *PyChemia*, https://github.com/MaterialsDiscovery/PyChemia (accessed Aug. 1, 2017).

(18) Kresse, G.; Hafner, J. Ab initio molecular dynamics for liquid metals. *Phys. Rev. B: Condens. Matter Mater. Phys.* **1993**, *47*, 558−561.

(19) Kresse, G.; Hafner, J. Ab initio molecular-dynamics simulation of the liquid-metal-amorphous-semiconductor transition in germanium. *Phys. Rev. B: Condens. Matter Mater. Phys.* **1994**, *49*, 14251−14269.

(20) Kresse, G.; Furthmüller, J. Efficiency of ab-initio total energy calculations for metals and semiconductors using a plane-wave basis set. *Comput. Mater. Sci.* **1996**, *6*, 15−50.

(21) Kresse, G.; Furthmüller, J. Efficient iterative schemes for ab initio total-energy calculations using a plane-wave basis set. *Phys. Rev. B: Condens. Matter Mater. Phys.* **1996**, *54*, 11169−11186.

DOI: 10.1021/acs.jctc.8b00404
J. Chem. Theory Comput. 2018, 14, 4455−4466

(22) Hobbs, D.; Kresse, G.; Hafner, J. Fully unconstrained noncollinear magnetism within the projector augmented-wave method. *Phys. Rev. B: Condens. Matter Mater. Phys.* **2000**, *62*, 11556−11570.
(23) Moriya, T. Theory of Magnetism of NiF_2. *Phys. Rev.* **1960**, *117*, 635−647.
(24) Ma, P.-W.; Dudarev, S. L. Constrained density functional for noncollinear magnetism. *Phys. Rev. B: Condens. Matter Mater. Phys.* **2015**, *91*, 054420.
(25) Ryee, S.; Han, M. J. Comparative study of DFT+*U* functionals for non-collinear magnetism. 2018, arXiv:cond-mat/802.10129; arXiv.org e-print archive. https://arxiv.org/abs/1802.10129.
(26) Blöchl, P. E. Projector augmented-wave method. *Phys. Rev. B: Condens. Matter Mater. Phys.* **1994**, *50*, 17953−17979.
(27) Kresse, G.; Joubert, D. From ultrasoft pseudopotentials to the projector augmented-wave method. *Phys. Rev. B: Condens. Matter Mater. Phys.* **1999**, *59*, 1758−1775.
(28) Gonze, X.; et al. Recent developments in the ABINIT software package. *Comput. Phys. Commun.* **2016**, *205*, 106.
(29) Gonze, X.; et al. ABINIT: First-principles approach to material and nanosystem properties. *Comput. Phys. Commun.* **2009**, *180*, 2582−2615. 40 {YEARS} {OF} CPC: A celebratory issue focused on quality software for high performance, grid and novel computing architectures.
(30) *Elk Code*,elk.sourceforge.net (accessed Mar. 1, 2018).
(31) Cooke, A. H.; Gehring, K. A.; Lazenby, R. The magnetic properties of NiF 2. *Proc. Phys. Soc., London* **1965**, *85*, 967.
(32) Hutchings, M. T.; Thorpe, M. F.; Birgeneau, R. J.; Fleury, P. A.; Guggenheim, H. J. Neutron and Optical Investigation of Magnons and Magnon-Magnon Interaction Effects in NiF_2. *Phys. Rev. B* **1970**, *2*, 1362−1373.
(33) Richards, P. L. Far-Infrared Magnetic Resonance in NiF_2. *Phys. Rev.* **1965**, *138*, A1769−A1775.
(34) Matarrese, L. M.; Stout, J. W. Magnetic Anisotropy of NiF_2. *Phys. Rev.* **1954**, *94*, 1792−1793.
(35) Singh, D. J., Papaconstantopoulos, D. A., Eds. *Electronic Structure and Magnetism of Complex Materials*, 1st ed.; Springer-Verlag: Berlin, Heidelberg, 2003; Vol. *54*.
(36) Zaanen, J.; Westra, C.; Sawatzky, G. A. Determination of the electronic structure of transition-metal compounds: 2p x-ray photo-emission spectroscopy of the nickel dihalides. *Phys. Rev. B: Condens. Matter Mater. Phys.* **1986**, *33*, 8060−8073.
(37) Strempfer, J.; Rütt, U.; Bayrakci, S. P.; Brückel, T.; Jauch, W. Magnetic properties of transition metal fluorides *M* F_2 (*M* = Mn, Fe, Co, Ni) via high-energy photon diffraction. *Phys. Rev. B: Condens. Matter Mater. Phys.* **2004**, *69*, 014417.
(38) Beineke, L. W.; Oellermann, O. R.; Pippert, R. E. The average connectivity of a graph. *Discrete Math.* **2002**, *252*, 31−45.
(39) Kota, Y.; Tsuchiura, H.; Sakuma, A. Ab-Initio Study on the Magnetic Structures in the Ordered Mn_3Pt Alloy. *IEEE Trans. Magn.* **2008**, *44*, 3131−3133.
(40) Krén, E.; Kádár, G.; Pál, L.; Sólyom, J.; Szabó, P.; Tarnóczi, T. Magnetic Structures and Exchange Interactions in the Mn-Pt System. *Phys. Rev.* **1968**, *171*, 574−585.
(41) Kubler, J.; Hock, K. H.; Sticht, J.; Williams, A. R. Density functional theory of non-collinear magnetism. *J. Phys. F: Met. Phys.* **1988**, *18*, 469.
(42) Sarneski, J. E.; Thorp, H. H.; Brudvig, G. W.; Crabtree, R. H.; Schulte, G. K. Assembly of high-valent oxomanganese clusters in aqueous solution. Redox equilibrium of water-stable Mn3O44+ and Mn2O23+ complexes. *J. Am. Chem. Soc.* **1990**, *112*, 7255−7260.
(43) GarciaCastro, A. C.; Romero, A. H.; Bousquet, E. Noncollinear magnetism in postperovskites from first principles: Comparison between CaRhO3 and NaNiF3. *Phys. Status Solidi B* **2015**, *252*, 689−694.

DOI: 10.1021/acs.jctc.8b00404
J. Chem. Theory Comput. 2018, 14, 4455−4466